Molecular Vision 2014; 20:215-230 <http://www.molvis.org/molvis/v20/215>
Received 11 November 2013 | Accepted 28 February 2014 | Published 3 March 2014

© 2014 Molecular Vision

Varied manifestations of persistent hyperplastic primary vitreous with graded somatic mosaic deletion of a single gene

Michelle N. Mary-Sinclair,[1] XiaoFei Wang,[2,3] Douglas J. Swanson,[4] Caroline Y. Sung,[1] Eneida A. Mendonca,[5] Kristen Wroblewski,[6] Shannon H. Baumer,[7] Dan Goldowitz,[4] Monica M. Jablonski,[2,3] Stephen X. Skapek[1]

[1]Department of Pediatrics, Division of Hematology/Oncology, University of Texas Southwestern Medical Center, Dallas, TX; [2]Department of Ophthalmology, University of Tennessee Health Science Center, Memphis, TN; [3]Department of Anatomy and Neurobiology, University of Tennessee Health Science Center, Memphis, TN; [4]Department of Medical Genetics, Centre of Molecular Medicine and Therapeutics, CFRI, University of British Columbia, Vancouver, BC, Canada; [5]Department of Pediatrics and Biostatistics and Medical Informatics, University of Wisconsin, Madison, WI; [6]Department of Health Studies, University of Chicago, Chicago, IL; [7]Department of Pediatrics, University of Chicago, Chicago, IL

Purpose: Persistent hyperplastic primary vitreous (PHPV) represents a developmental eye disease known to have diverse manifestations ranging from a trivial remnant of hyaloid vessels to a dense fibrovascular mass causing lens opacity and retinal detachment. PHPV can be modeled in mice lacking individual genes, but certain features of such models differ from the clinical realm. For example, mice lacking the *Arf* gene have uniformly severe disease with consistent autosomal recessive disease penetrance. We tested whether the graded somatic loss of *Arf* in a subset of cells in chimeric mice mimics the range of disease in a non-heritable manner.

Methods: Wild type ↔ *Arf*$^{-/-}$ mouse chimeras were generated by morulae fusion, and when the mice were 10 weeks old, fundoscopic, slit-lamp, and histological evaluations were performed. The relative fraction of cells of the *Arf*$^{-/-}$ lineage was assessed with visual, molecular genetic, and histological analysis. Objective quantification of various aspects of the phenotype was correlated with the genotype.

Results: Sixteen chimeras were generated and shown to have low, medium, and high contributions of *Arf*$^{-/-}$ cells to tail DNA, the cornea, and the retinal pigment epithelium (RPE), with excellent correlation between chimerism in the tail DNA and the RPE. Phenotypic differences (coat color and severity of eye disease) were evident, objectively quantified, and found to correlate with the contribution of *Arf*$^{-/-}$ cells to the RPE and tail-derived DNA, but not the cornea.

Conclusions: Generating animals composed of different numbers of *Arf*$^{-/-}$ cells mimicked the range of disease severity observed in patients with PHPV. This establishes the potential for full manifestations of PHPV to be caused by somatic mutations of a single gene during development.

During ocular development, the hyaloid vascular system (HVS) in the primary vitreous nourishes the developing vitreous and lens [1,2]. The HVS regresses in later stages of development to leave the largely acellular mature vitreous space. Vision is compromised when the process goes awry in certain ocular diseases such as persistent hyperplastic primary vitreous (PHPV), also known as persistent fetal vasculature (PFV) [1,3]. PHPV treatment is largely limited to surgical intervention (such as lensectomy, vitrectomy, membranectomy) to prevent late sequelae such as glaucoma or phthisis, but these approaches have less capacity to restore vision when the disease is severe [4,5]. Relatively little is known about the molecular pathogenesis of PHPV/PFV. The rare occurrence of familial disease has implied a genetic cause [6-8], and certain molecular genetic abnormalities have been correlated with cases of PHPV that are accompanied by other developmental defects [9-11].

To gain more insight into possible disease-causing aberrations, we and others have leveraged mouse models to elucidate the fundamental processes driving primary vitreous maturation and HVS regression. It is clear that disrupting cellular or genetic mechanisms that promote endothelial cell apoptosis can lead to persistence of the hyaloid vessels. Examples include loss of Wnt7b signals in macrophage-like hyalocytes [12], and the absence of Angiopoietin 2 [13,14] or p53 [15,16], which may be linked to endothelial cell apoptosis in the postnatal period [16]. HVS regression is also blocked by hyperplasia of perivascular cells in the primary vitreous. This occurs in mice with deficient Tgfβ signaling [17-19], ectopic expression of the pseudorabies virus protein IE180 [20], deregulated vascular endothelial growth factor (Vegf) [21], and the absence of the *Arf* tumor suppressor. In this last model, the *Arf* gene product, p19^{Arf}, blocks proliferation signals stemming from Pdgfrß [22,23]. The resulting

Correspondence to: Stephen X. Skapek, Department of Pediatrics, Division of Hematology/Oncology, University of Texas Southwestern Medical Center, 5323 Harry Hines Blvd, MC 9063, Dallas, TX, 75390; Phone: (214) 648-3081; FAX: (214) 648-3122; email: Stephen.Skapek@UTSouthwestern.edu

hyperplastic perivascular cells provide trophic factors, such as Vegf, which may impede the HVS involution [24].

We have focused on the *Arf* model of primary vitreous hyperplasia because *Arf* is normally expressed in perivascular cells enveloping the mouse HVS, and the robust phenotype recapitulates many aspects of severe PHPV [22,24]. Human *ARF* abnormalities have not yet been described in patients with PHPV, and two features of the human disease are not reflected in the *Arf* $^{-/-}$ model. First, disease penetrance is essentially complete in the mouse, clearly tracking as an autosomal recessive trait. Second, uniformly severe disease develops in both eyes in *Arf* $^{-/-}$ mice, whereas human disease manifestations vary widely and are often unilateral [1,3]. We considered that if the disease were due to a somatic mutation of a critical gene in only a subset of cells in development, it might not be heritable. Further, the disease manifestations might also vary, perhaps in proportion to the number of cells lacking the critical gene. We previously showed that mosaic mice composed of a mixture of *Arf* wild type and *Arf* $^{-/-}$ cells displayed primary vitreous hyperplasia at birth, proving that p19^{Arf} uses primarily cell-intrinsic mechanisms to control accumulation of Pdgfrß-expressing cells in the primary vitreous [25]. Thus, most of the cells that populate the PHPV tissue at birth are drawn from the *Arf* $^{-/-}$ pool. We conducted the current analyses to test whether the somatic mosaic loss of *Arf* could lead to the full "clinical" manifestations of PHPV and whether the relative proportion of *Arf*-deficient cells in the chimeric animal correlated with disease severity.

METHODS

Generating chimeric mice: Chimeric mice composed of wild type and *Arf* $^{-/-}$ cells (wild type ↔ *Arf* $^{-/-}$ chimeras) were generated by morulae fusion at embryonic day (E) 2.5, essentially as previously described [25,26]. Briefly, superovulated wild type and *Arf* $^{-/-}$ females were mated to males of the same genotype for collection of four- to eight-cell stage embryos, which were subsequently treated with gentle Pronase digestion, aggregated with an embryo of the other genotype, cultured overnight for successful fusion, and implanted into the uterine horns of pseudo-pregnant female hosts. We used *Arf* $^{lacZ/lacZ}$ (referred to throughout as *Arf* $^{-/-}$) mice in which *lacZ* cDNA replaces the coding sequence for *Arf* exon 1β to generate a null allele [19] and *Arf* wild type mice, expressing green fluorescent protein (Gfp) under control of the chicken β-actin promoter. Chimeric mice were euthanized at 68 days of age for the experimental studies. All animal experiments were approved by the St. Jude Children's Research Hospital and the University of Tennessee Health Science Center Animal Care and Use Committees (where the work was performed) and comply with the Office of Laboratory Animal Welfare Public Health Service Policy on Humane Care and Use of Laboratory Animals.

Assessment of degree of chimerism: The relative contribution of wild type and *Arf* $^{-/-}$ cells to chimeric animals was assessed in three ways. First, digital photomicrographs documented coat color. The *Arf* wild type mice were albino; the *Arf* $^{-/-}$ mice were of mixed C57Bl/6 × 129/Sv lineage and uniformly had agouti coat color. Without knowledge of molecular genotyping, individual mice were scored as being mostly wild type (white), mostly *Arf* $^{-/-}$ (agouti), or mixed. Second, molecular genotyping was performed using polymerase chain reaction (PCR) on tail-derived genomic DNA with allele-specific primers: 5'-TTG AGG AGG ACC GTG AAG CCG-3' (wild type); 5'-GTG AGG CCG CCG CTG AGG GAG TA-3' (wild type and *Arf* $^{-/-}$); 5'-CCA GCT GGC GAA AGG GGG ATG TG-3' (*Arf* $^{-/-}$). PCR amplification was carried out for 30 cycles at 94 °C (1 min), 64 °C (1 min), and 72 °C (2 min). Following electrophoresis and imaging of PCR products on ethidium bromide-stained agarose gel, relative band intensity was assessed using Quantity One 1-D Analysis Software (BioRad, Hercules, CA). Finally, eyes removed from CO_2-euthanized animals were fixed in 4% paraformaldehyde, infused with 30% sucrose, and embedded in tissue freezing medium (TBS). Gfp expression (marking the *Arf* wild type cells) was evaluated using direct fluorescence microscopy on 5 µm thick, midline, anterior-posterior sections using a BX60 light/fluorescence microscope (Olympus, Tokyo, Japan) with an EGFP bandpass filter set (Chroma, Bellows Falls, VT). Eyes from non-chimeric *Arf* $^{-/-}$ and *Arf* wild type mice, expressing Gfp from the chicken β-actin promoter, served as negative and positive controls, respectively. Relative wild type and *Arf* $^{-/-}$ contribution was expressed as a percentage of the total.

Assessment of phenotype severity: Ocular disease was assessed in 13 chimeric mice in which genomic DNA had been successfully amplified and quantified and in the controls. Mice were sedated with intraperitoneal injection of Avertin (tribromoethanol; 0.35 ml). The anterior segment, including the posterior lens, was examined with a slit-lamp biomicroscope (Carl Zeiss, Oberkochen, Germany). Pupils were then dilated using cyclopentolate HCl (0.2%) and phenylephrine (1%). The fundi were examined with indirect ophthalmoscopy. Photographs were taken using a Kowa Genesis (Torrance, CA) small animal fundus camera equipped with a 90 D condensing lens (Volk, Mentor, OH) [27], and 160T slide film (Kodak, Rochester, NY) was used for photographic documentation. One of the authors (XFW) provided written descriptions of the ocular findings;

subsequently, the eyes were scored as having a low, medium, or high degree of disease independently of knowledge of the mouse genotype or pathology findings.

Disease severity was also determined by using hematoxylin and eosin stained sections of mouse eyes. Sections were scored for the presence or absence and the size of a retrolental mass (RLM) without knowledge of the genotype. Representative photomicrographs were obtained using a SPOT camera and Photoshop CS3 software (Adobe Systems, San Jose, CA).

Statistical analyses: The relative contribution of wild type and *Arf*$^{-/-}$ cells was calculated based on a) the PCR results of genomic DNA, b) fluorescence microscopy detection of Gfp in the corneal epithelium, and c) light microscopy detection of pigmented cells in the retinal pigment epithelium (RPE); degree of chimerism was expressed as a percentage of the total. Pearson correlation coefficients were calculated to examine the association among the three methods for measuring the degree of chimerism (DNA, RPE, and cornea). Correlation analysis was also performed to determine the association between the degree of chimerism and the size of the retrolental mass as measured in the number of pixels. The nonparametric Kruskal-Wallis test and the trend test as described by Cuzick [28] were used to assess the relationship between coat color (light, mixed, or dark) or disease severity based on exam findings (low, moderate, or high) and the chimerism percentage. Because an animal could contribute more than one eye to the analysis, this natural clustering in the data was accounted for in the analysis in one of two ways: 1) The average of the two eyes for each animal was used, or 2) individual eyes were included using linear regression methods with an adjustment to the standard error to account for the clustering. A p value < 0.05 was considered statistically significant. Last, the intraclass correlation coefficient (ICC) was calculated to examine the amount of variability in the RPE and cornea values due to inter- versus intra-mouse differences. An ICC of 1 would indicate that all the variability was completely due to inter-mouse differences (i.e., the RPE and cornea values for eyes in the same mouse were in perfect agreement). All analyses were performed using Stata, Version 10 (StataCorp, College Station, TX).

RESULTS

Fused morulae, implanted in the uteri of four pseudopregnant female mice resulted in 16 wild type ↔ *Arf*$^{-/-}$ chimeric pups and nine *Arf*$^{-/-}$ control weaned pups. Visual inspection of the coat revealed four pups with mostly white coats, five with mostly agouti coats, and seven judged to have approximately equal mixing of coat color (Figure 1A-C). Because the wild type mice and *Arf*$^{-/-}$ mice had white and agouti coats, respectively, these data indicated that the *Arf*$^{-/-}$ contribution to these chimeras ranged from relatively low to high.

A semiquantitative PCR assay (see Methods) assessed the relative ratio of wild type and *Arf*$^{-/-}$ alleles in genomic DNA derived from the tail biopsy samples. Because the wild type allele was amplified more efficiently (Figure 1D, lane 2), the relative intensity of each band was normalized to *Arf*$^{+/-}$ heterozygous DNA, which was amplified in parallel. Quantitative analysis from the 13 chimeric animals with measurable DNA indicated that the contribution of wild type and mutant *Arf*$^{-/-}$ cells in the tail-derived DNA ranged from nearly all wild type (Figure 1E, lane D) to nearly all *Arf*$^{-/-}$ (Figure 1E, lane F).

We next quantified the relative contribution of wild type and *Arf*-deficient cells to individual tissues of the eye. Direct green fluorescence was used to assess chimerism in the cornea. In this case, the total length of the corneal epithelium was determined using 4',6-diamidino-2-phenylindole dihydrochloride (DAPI)–stained images (Figure 2B,D,F). The total length of green fluorescence versus non-green fluorescence (Figure 2A,C,E) was calculated to determine the relative number of wild type and *Arf*$^{-/-}$ cells, respectively. To assess the RPE, we took advantage of the fact that the *Arf* wild type mice were albino. Hematoxylin and eosin stained eyes showed regions of the RPE that had or lacked pigment (Figure 2G,H, arrowhead versus arrows) and therefore were derived from the *Arf*$^{-/-}$ or wild type lineage, respectively. The relative linear distance of pigmented versus non-pigmented RPE was calculated from these images. Midline sections were of sufficient quality to allow quantitative analysis of 16 eyes taken from nine animals (Figure 2I). The degree of chimerism in the cornea and the RPE varied widely across the cohort, as it did in the tail-derived DNA and coat color analysis. However, the intraclass correlation coefficient for the RPE was 0.92 and for the cornea was 0.77, suggesting that variation between two eyes in the same mouse was less than the mouse-to-mouse differences.

We previously showed that the wild type and *Arf*$^{-/-}$ contribution in tail-derived DNA, cornea, and RPE correlate with each other in newborn pups [25]. Similarly, linear regression analyses showed that the *Arf*$^{-/-}$ lineage contribution to the RPE correlated well with its contribution to tail-derived DNA ($p<0.001$) (Figure 3A,D) but less well when the tail-derived DNA ($p = 0.014$) and the RPE ($p = 0.010$) were compared to the cornea (Figure 3B,C,E,F).

We also tested whether the degree of chimerism correlated with various aspects of the mouse phenotype. We first compared the relative *Arf*$^{-/-}$ content to the coat phenotype.

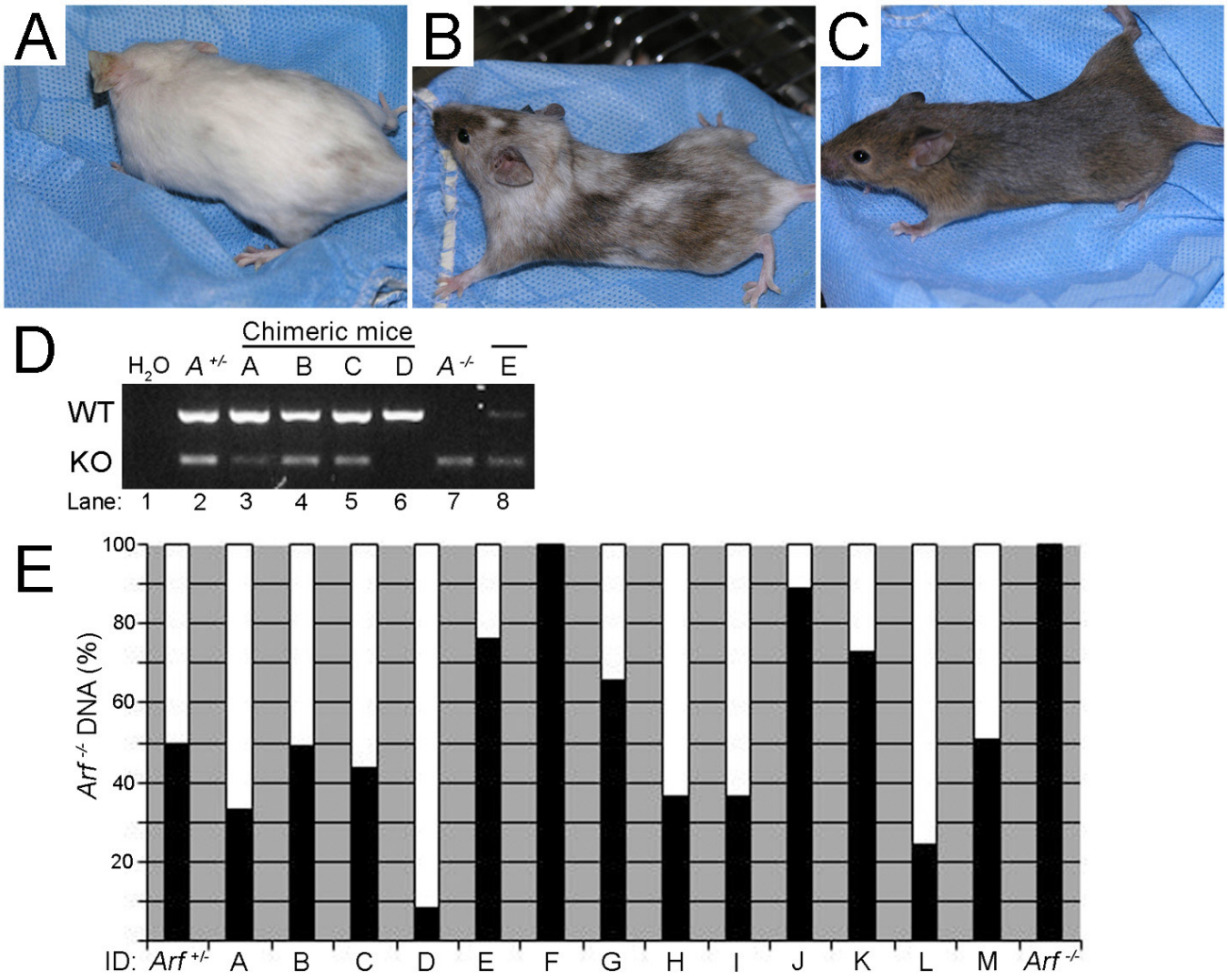

Figure 1. Chimeric mice are composed of varying degrees of wild type and *Arf* $^{-/-}$ cells. **A-C**: Representative photos of 10-week-old mice that have low (**A**), medium (**B**) and high (**C**) amounts of *Arf* $^{-/-}$ cells based on coat color. **D** and **E**: Representative photograph of ethidium bromide-stained gel of PCR amplification of wild type (WT) and targeted (KO) *Arf* alleles from tail-derived DNA (**D**) and their quantification (**E**). Black and white bars represent *Arf* $^{-/-}$ and wild type genotype, respectively. *Arf* $^{+/-}$ and *Arf* $^{-/-}$ are included as controls. Letters designating individual animals are consistent throughout the manuscript.

Regardless of whether it was based on genomic DNA from the tail biopsy or the assessment of the RPE, the average *Arf* $^{-/-}$ content increased step-wise in mice that were judged to have mostly white, mixed, or mostly agouti coats (Figure 4A,B). In contrast, coat color did not correlate with chimerism based on the cornea analysis (Figure 4C; also see summary in Table 1).

As with the coat color assessment, ocular disease manifestations varied across the cohort of chimeric mice (Figure 5). Disease manifestations were felt to be of low, moderate, and high severity based on slit-lamp and fundoscopic evaluations, but all chimeric mice had some evidence of disease, based on the presence of a retrolental membrane on the slit-lamp exam or visual evidence of remnants of the hyaloid vasculature in the vitreous on the fundus exam (Figure 5B). In some cases, the vitreous membrane was darkly pigmented whereas, in other cases, pigmentation was minimal or absent on "clinical" examination. The slit-lamp exam findings ranged from the lens being essentially normal in two eyes to having the posterior surface completely covered by a retrolental membrane. The fundus findings ranged from observing small remnants of the hyaloid vessels to the presence of a retrolental mass fully obscuring the fundus. Disease severity assessed with the slit-lamp exam correlated with the severity on the fundoscopic exam in 25 of 26 eyes. Further, disease

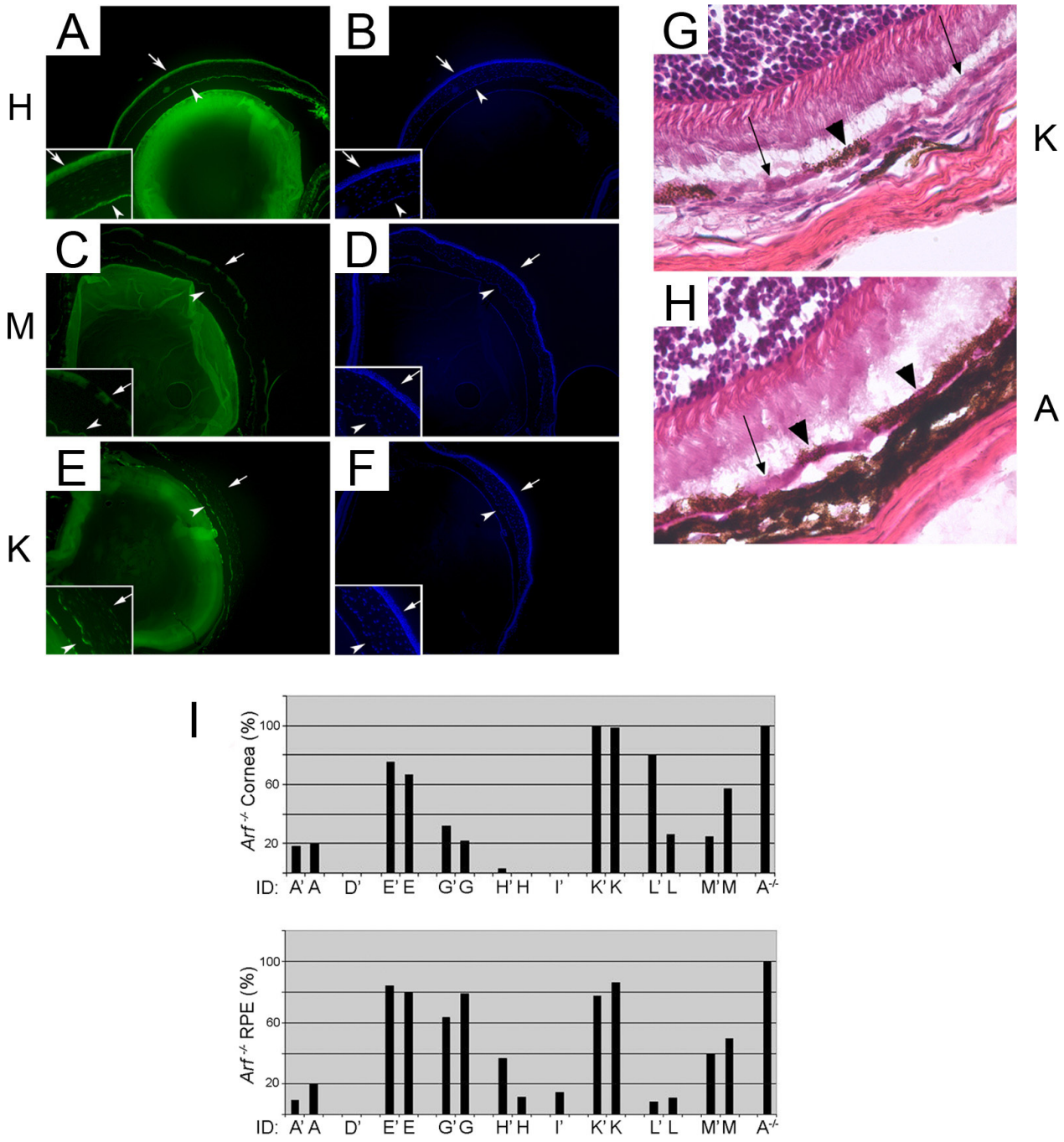

Figure 2. Eyes from chimeric mice are composed of varying degrees of wild type and *Arf*$^{-/-}$ cells. **A-H**: Representative photomicrographs of fluorescence (**A-F**) or light microscopic images of hematoxylin and eosin stained sections (**G** and **H**). Letters (H, M, K, A) to the side of images indicate the animal ID. Green fluorescence (**A**, **C**, **E**) denotes wild type lineage; 4',6-diamidino-2-phenylindole dihydrochloride (DAPI) staining (**B**, **D**, **F**) shows all nuclei in sections. Arrows and arrowheads show the corneal epithelium and endothelium, respectively (**A-F**) and wild type (non-pigmented) and *Arf*$^{-/-}$ (pigmented) RPE, respectively (**G** and **H**). Insets (**A-F**) show higher magnification. **I**: Absolute quantification of the relative contribution from the *Arf*$^{-/-}$ lineage in the cornea and the RPE, represented as percentage of total. Letters and letter primes distinguish individual eyes from the same chimeric animal.

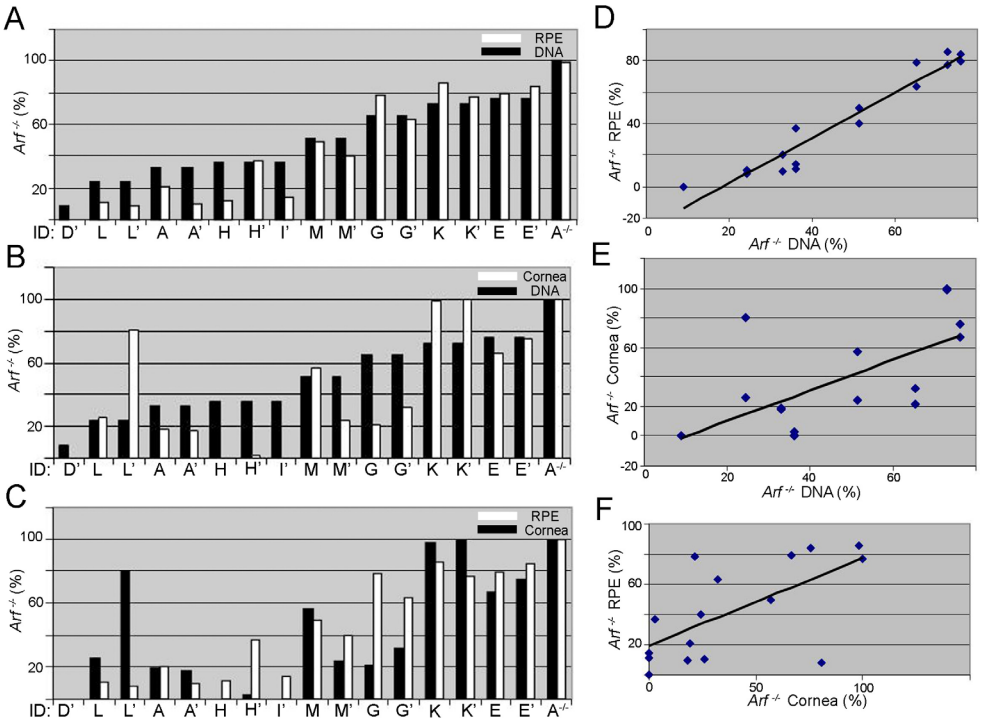

Figure 3. The percentage of *Arf* $^{-/-}$ lineage in the tail-derived DNA and retinal pigment epithelium (RPE) correlate with each other, but not as well with the corneal epithelium. **A**–**C**: Quantitative analysis of individual eyes depicts the percent *Arf* $^{-/-}$ genotype for the RPE, tail DNA, and the cornea. Black and white bars denote specific tissue as indicated on individual charts. Letters and letter primes denote individual eyes from the same chimeric animal. **D**–**F**: Linear regressions show excellent correlation of genotype in the RPE compared to tail-derived DNA (Pearson correlation coefficient = 0.97; p<0.001; **D**), and a weaker correlation when DNA (**E**) or RPE (**F**) is compared to the cornea (Pearson correlation coefficients = 0.63 [p = 0.014] and 0.64 [p = 0.010], respectively).

scoring was concordant in both eyes of 11 of 13 (slit-lamp) and 12 of 13 (fundoscopic) animals.

The severity of eye disease was also assessed microscopically by scoring the midline sections for the presence or absence of a retrolental mass and by measuring the size of the mass (Figure 6). We detected a retrolental mass in the midline sections of eyes from all *Arf* $^{-/-}$ animals, whereas a mass was detected in only 62.5% of the chimeric eyes. We noted that 11 of 12 retrolental masses from chimeric mice contained densely pigmented cells, indicating their derivation from the non-albino, *Arf* $^{-/-}$ lineage (Figure 6C-F). None of the eyes with low disease severity on the fundus exam had pathological evidence of a retrolental mass. In contrast, 67% and 100% of the eyes judged to have moderate or severe fundoscopic evidence of disease, respectively, had a retrolental mass on histological assessment. The average size of the retrolental mass was smaller in the chimeric animals as compared to the *Arf* $^{-/-}$ eyes (Figure 6J).

Last, we determined whether the severity of ocular disease correlated with the contribution of *Arf* $^{-/-}$ cells in the animal. The quantity of *Arf* $^{-/-}$ cells in the tail-derived DNA and RPE correlated with the ocular disease severity based on either fundoscopic or slit-lamp exams in chimeric mice (Figure 7A,B; additional data not shown). Greater *Arf* $^{-/-}$ contribution to these tissues also correlated with the presence of a larger retrolental mass size on histological analysis (Figure 8A,B). The roughly linear relationship between the retrolental mass size and *Arf* $^{-/-}$ contribution to these tissues speaks to the cell-intrinsic mechanism by which p19^{Arf} controls the accumulation of primary vitreous cells [25]. However, differences in *Arf* $^{-/-}$ content in the cornea did not correlate with ocular disease severity (Figure 7C) or with larger retrolental mass size (Figure 8C; also see summary in Table 2).

DISCUSSION

In general, PHPV pathogenesis centers on either the disruption of proapoptotic pathways needed to directly promote endothelial cell regression in the HVS or the override of mechanisms for preventing hyperplasia of perivascular cells enveloping the hyaloid vessels. Numerous mouse models support the concept that this disease has a genetic basis [12,15-19,21,22,24], and in most, the disease exhibits an autosomal dominant or recessive inheritance pattern with a phenotype penetrance that can be complete. In that regard, though, such models fail to reflect certain clinical features of human PHPV, including the fact that it is only rarely reported to be heritable [6-8,29].

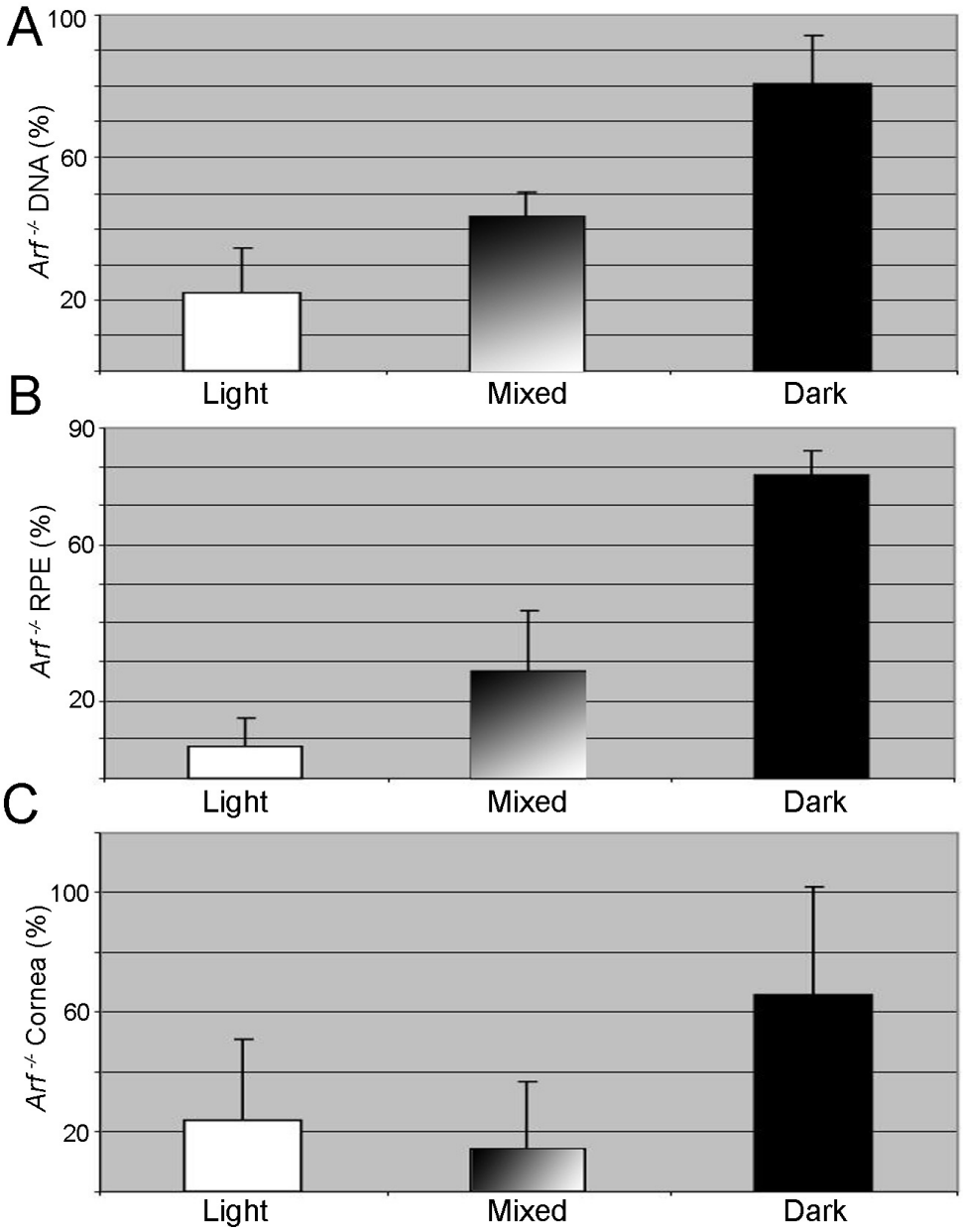

Figure 4. The coat color phenotype correlates with the quantitative measurement of the *Arf* $^{-/-}$ lineage contribution to chimera. Charts display the average *Arf* $^{-/-}$ content in the tail-derived DNA (**A**), retinal pigment epithelium (RPE) (**B**), and cornea (**C**) in chimeric animals with light, mixed, and dark coats as indicated; error bars indicate standard deviation. The non-parametric trend test was used to account for the trend in color, and showed a significant correlation of coat color with the tail-derived DNA ($p = 0.001$) and RPE ($p = 0.011$), but not with the cornea ($p = 0.155$).

In the case of *Arf* loss as a mouse model for PHPV, Pdgfrß-dependent signals drive excess proliferation of vascular mural cells enveloping the hyaloid stalk and vasa hyaloidea propria in the posterior eye [23,24]. Thus, this model principally models primary vitreous hyperplasia that derails the involution of only the posterior components of the hyaloid vasculature. The usual clinical scenario for patients with PHPV, though, contrasts three features of the *Arf* $^{-/-}$ model: Ocular disease in the *Arf* $^{-/-}$ mouse is heritable with complete penetrance, it is consistently bilateral and severe, and it is associated with cancer susceptibility. The incongruence between the clinical specimen and this model can be mostly eliminated if we consider that PHPV might be caused by somatic loss of human *ARF*. First, although we did not formally test whether the PHPV-like phenotype is heritable in the mouse chimeras we generated, we recently demonstrated that mouse *Arf* deletion in cells derived from the *Wnt1*-expressing neural crest results in PHPV [30]. Thus, although there is as yet no evidence from clinical specimens, one could envision that human *ARF* disruption in just the neural crest might be sufficient for PHPV. As a somatic mutation, the germ line could remain unaffected, and the disease would not be heritable.

Table 1. Summary of Arf null cell contribution to various tissues in chimeric mice.

ID	Coat color	Tail DNA (% Arf null)	Eye	Cornea (% Arf null)	RPE (% Arf null)
D	Light	8.9	R	-	-
			L	0	0.5
L	Light	24.3	R	25.8	10.7
			L	80.6	8.3
A	Light	33	R	19	20.4
			L	17.9	9.5
H	Mixed	36.1	R	0.2	11.5
			L	2.7	36.9
I	Mixed	36.2	R	-	-
			L	0	0.1
C	Mixed	43.6	R	-	-
			L	-	-
B	Mixed	49.2	R	-	-
			L	-	-
M	Mixed	51.3	R	56.8	49.6
			L	24.1	40.1
G	Dark	65.3	R	21.4	78.4
			L	32.2	63.4
K	Dark	72.9	R	-	-
			L	100	77
E	Dark	76	R	66.8	79.3
			L	75.4	84.3
F	Dark	99.9	R	-	-
			L	-	-
J	Dark	88.6	R	-	-
			L	-	-

Second, by varying the number of *Arf* $^{-/-}$ cells in the chimeric mouse, we recapitulated the wider spectrum of disease that occurs in the clinical setting. In the 26 chimeric eyes we examined "clinically," nearly one third had minimal evidence of disease. In some cases, the "clinical" exam findings were essentially normal or displayed only a small retrolental membrane and persistence of the hyaloid stalk exactly modeling milder forms of the disease. Beyond demonstrating that disease severity varied with the relative number of *Arf*-deficient cells, we also occasionally generated chimeric mice with little or no detectable disease in one of the eyes, which may reflect unilateral distribution of *Arf* $^{-/-}$ cells in the fused morulae. One could also envision unilateral defects due to mitotic recombination later during embryogenesis in a human heterozygous "carrier" of a single mutant *ARF* allele. Mouse *Arf* is expressed within the eye from the point when HVS vessels are initially forming (approximately E12.5), and the expression persists until the vessels begin to regress in the first postnatal week [22,24]. Thus, this would represent the developmental window in which disrupting *ARF* or its expression could cause unilateral disease, perhaps with even less severe manifestations.

Third, one might expect cancer susceptibility if somatic *ARF* deletion contributes to PHPV, but an association between PHPV and cancer has not been described. It is widely accepted that p19^{Arf} suppresses tumor formation by exerting cell-intrinsic control over cell proliferation and apoptosis in nascent cancer cells [31,32], and we proved that this protein controls the accumulation of Pdgfrß-expressing cells in the primary vitreous in a cell autonomous manner [25]. As has been observed in individuals with somatic deletion of other tumor suppressors, including p53 [33], human *ARF* $^{-/-}$ cells should be at risk for neoplastic growth in a chimeric setting.

A

	Fundus			
Slit Lamp	L	M	H	Total
L	7	1	0	8
M	0	6	0	6
H	0	0	12	12
Total	7	7	12	26

B

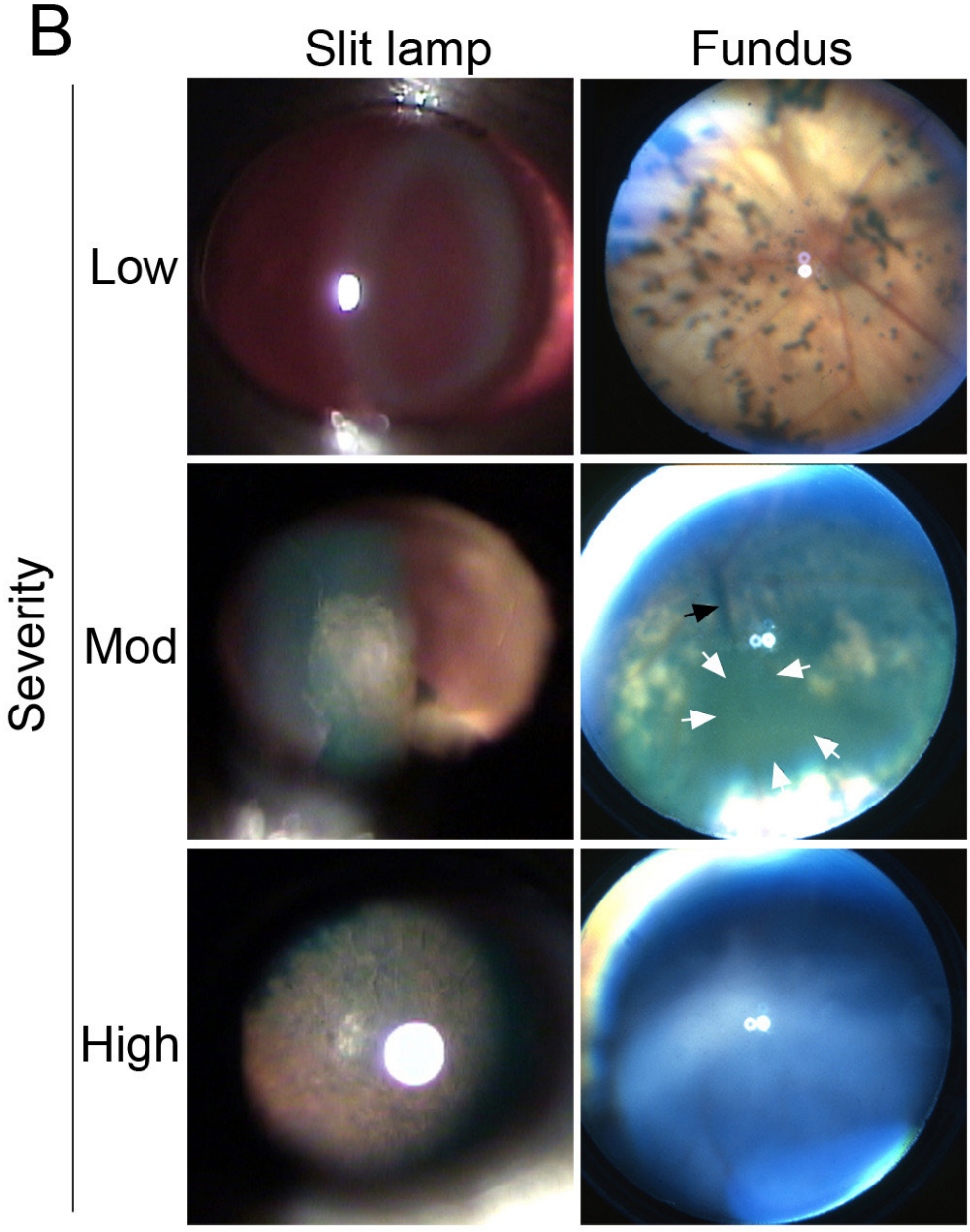

Figure 5. Ophthalmoscopy evaluation of chimeric mice shows a range of disease severity. **A**: Tabulation showing the number of eyes with low, moderate, and high degree of disease (L, M, H, respectively) based on slit-lamp and fundoscopic evaluations. Note that two eyes included in the Low category were felt to be normal by visual inspection. **B**: Representative photographs of eyes used to generate data in (**A**). The black arrow indicates a hyaloid vessel. White arrows denote focal lens opacity.

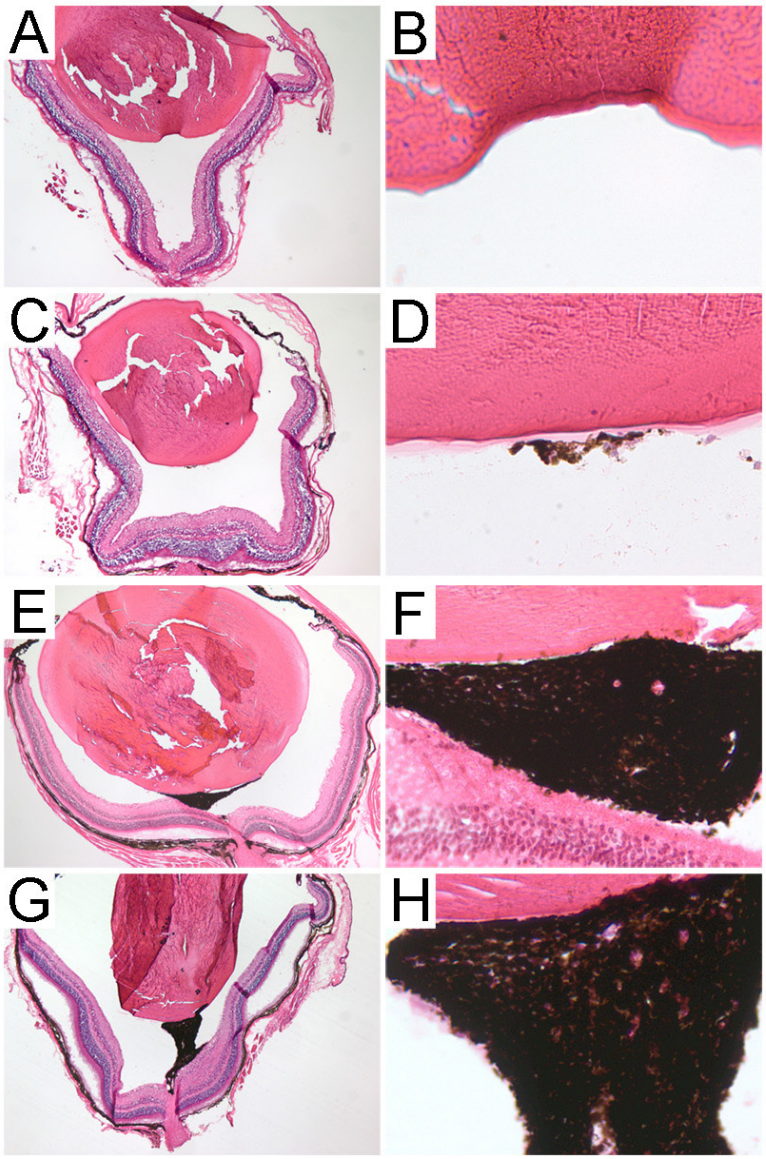

I

Mass ?	Yes	No	Total
Chimera	10	6	16
Arf $^{-/-}$	6	0	6

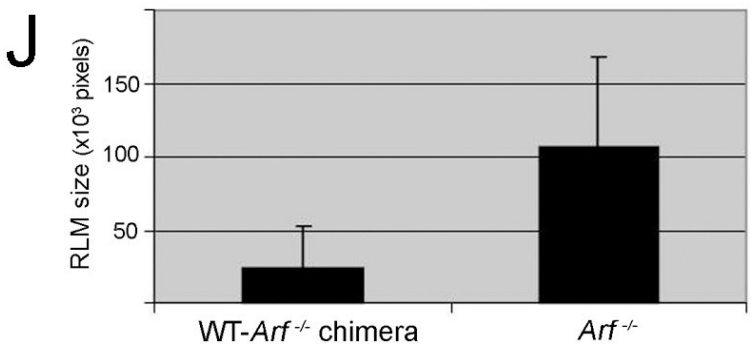

Figure 6. Histological studies reveal a range of disease severity in the eyes of chimeric mice. **A-H**: Representative photomicrographs of hematoxylin and eosin stained sections of chimeric (**A**, **C**, **E**) and *Arf* $^{-/-}$ (**G**) eyes show a retrolental mass (RLM; shown at higher magnification in **B**, **D**, **F**, **H**) with dense accumulation of pigmented cells. **I**: Tabulation of whether a RLM is present in the midline sections of individual eyes. **J**: Mean size of the RLM is larger in *Arf* $^{-/-}$ mice than in chimeric mice ($p = 0.031$). Error bars depict standard deviation.

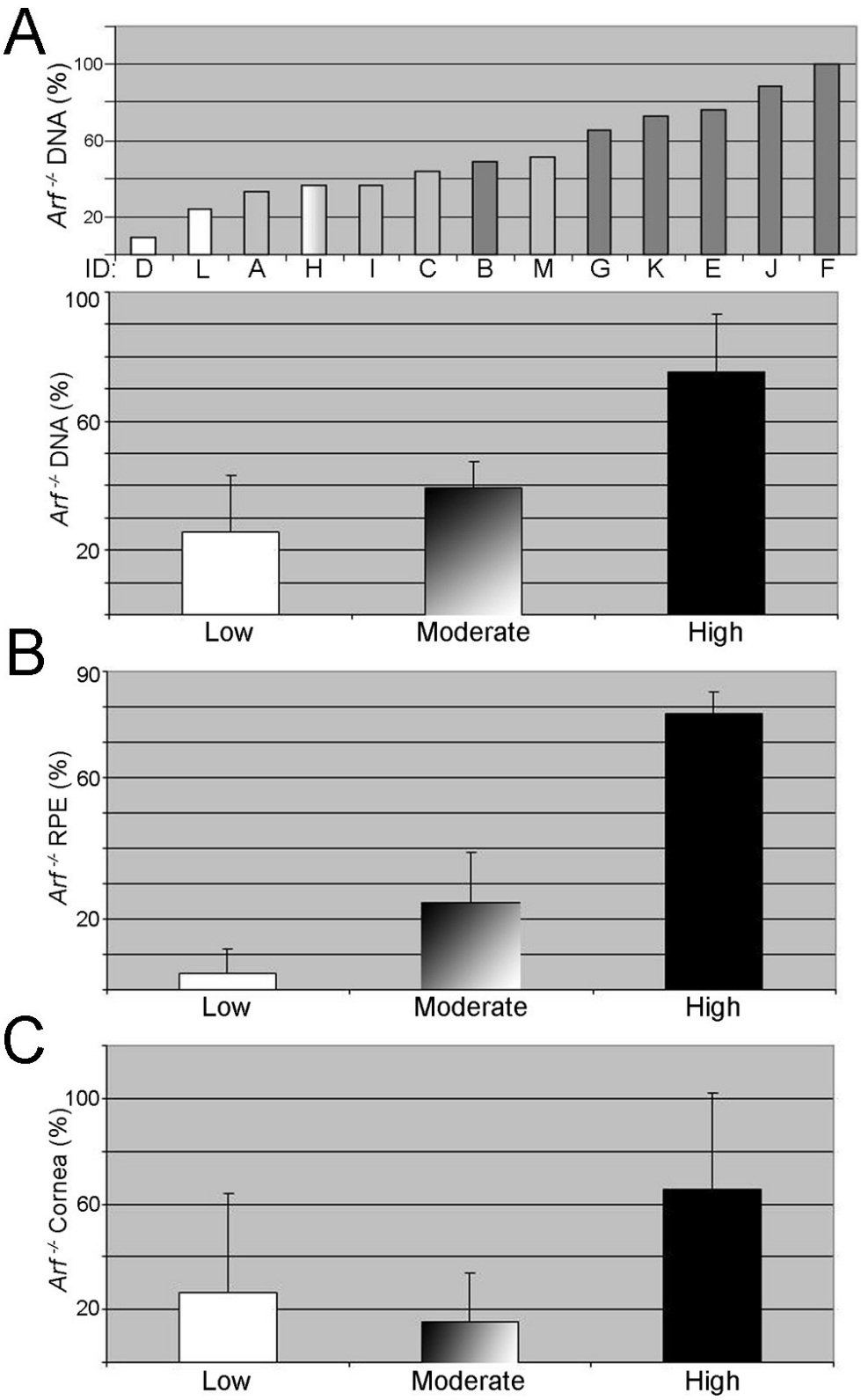

Figure 7. Ocular disease severity, based on fundoscopic findings, correlates with *Arf* $^{-/-}$ contribution to DNA and the retinal pigment epithelium (RPE). Relative amount of *Arf* $^{-/-}$ cells in individual eyes (top chart in **A**; letters denote individual animals consistent throughout the manuscript) and average *Arf* $^{-/-}$ contribution (bottom chart in **A**, and **B** and **C**) in eyes noted prospectively to have low, moderate, or high disease severity. Shaded bars (top chart in **A**) show individual eyes with low (white), moderate (gray), and high (dark gray) disease severity. Note that H has one eye each with low and moderate eye disease. The non-parametric trend test is significant in **A** and **B** ($p = 0.004$ and $p = 0.008$, respectively) but not significant in **C** ($p = 0.159$).

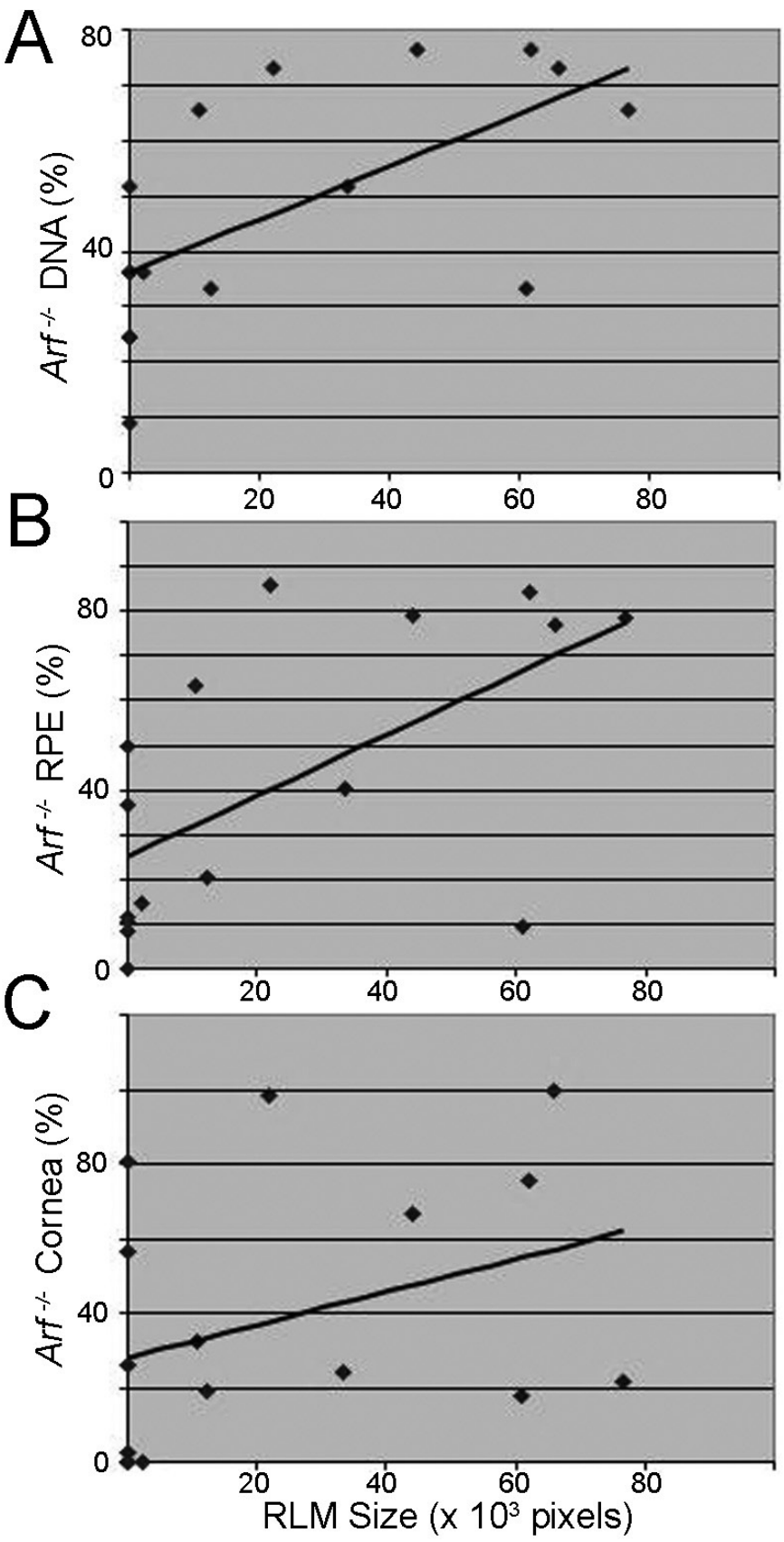

Figure 8. Histological assessment of disease severity correlates with degree of chimerism. Linear regression of the number of pixels in the retrolental mass (RLM) versus *Arf* $^{-/-}$ contribution, accounting for clustering of the eyes, showed good correlation for tailed-derived DNA (**A**) and the retinal pigment epithelium (RPE) (**B**) (Pearson correlation coefficients = 0.63 [p = 0.001] and 0.61 [p = 0.007], respectively), but not the cornea (**C**; Pearson correlation coefficient = 0.35, p = 0.101).

Table 2. Summary of ocular phenotype in chimeric mice.

ID	Tail DNA (% Arf null)	Eye	"Clinical" findings	Eye Grade	RLM
D	8.9	R	lightly increased density in the center	-	-
		L	normal	L	N
L	24.3	R	small mass behind the lens	L	N
		L	normal	L	N
A	33	R	medium sized pigmented membrane	M	Y
		L	pigmented membrane covers 1/4 of the area	M	Y
H	36.1	R	small area of increased density	L	N
		L	pigmented membrane	M	N
I	36.2	R	increased density in small area in the center	-	-
		L	pigmented membrane at the lower half	M	Y
C	43.6	R	lightly increased density in the center	-	-
		L	lightly increased density in the center	-	-
B	49.2	R	medium sized pigmented membrane	-	-
		L	medium sized pigmented membrane	-	-
M	51.3	R	dense circle in the center	M	N
		L	pigmented membrane occupying 2/3 of the area	M	Y
G	65.3	R	pigmented membrane	H	Y
		L	fibrous membrane at the lower half	H	Y
K	72.9	R	big pigmented membrane	-	Y
		L	big pigmented membrane	H	Y
E	76	R	big pigmented membrane	H	Y
		L	big pigmented membrane	H	Y
F	99.9	R	opaque lens, some pigmentation behind the lens	-	-
		L	1/3 is covered by pigmented membrane, fibrous	-	-
J	88.6	R	big pigmented membrane	-	-
		L	big fibrous membrane	-	-

However, two important points should be noted. First, there are few reports of *ARF* haploinsufficiency in the human germ line, and *ARF* disruption is often accompanied by deletion of the overlapping *INK4A* tumor suppressor gene [34-36]. Second, it is commonly felt that *INK4A* has greater tumor suppressor activity than *ARF* in humans [37]. Even considering disruption of both genes, germ line haploinsufficiency at this locus does not lead to wide cancer susceptibility similar to that described for the *p53* mutation [34-36]. This suggests that tumor susceptibility in the absence of *ARF/INK4A* is strongly influenced by cell or developmental contexts. This is analogous to cancer susceptibility in the setting of germ-line *RB* haploinsufficiency. Loss of a second allele leads to retinoblastoma formation with essentially complete penetrance, but the cancer risk is largely (though not exclusively) limited to the retina, with the retina tumor risk diminishing after the first 2 years of life [38]. For these reasons, somatic loss of just *ARF* in a narrowly defined lineage during human eye development may not unmask a clinically relevant cancer predisposition.

For somatic deletion of human *ARF* to represent a tenable pathogenetic mechanism for PHPV, both *ARF* alleles must be disrupted in a cell lineage ultimately giving rise to perivascular cells in the primary vitreous (likely, the neural crest, based on our studies of *Wnt1-Cre, Arf* $^{fl/fl}$ mice [30]); and the deletion must occur within the critical developmental window alluded to. This concept is not without precedent because an heritable retinoblastoma forms when a second *RB* gene mutation occurs during embryonic or early postnatal development in a child with germ-line *RB* haploinsufficiency [38]. The *Arf* locus seems particularly prone to recombination events leading to gene deletions in cultured fibroblasts [39], in mouse models of cancer [40,41], and in certain human tumors

[42,43]. High-density arrays for detecting single nucleotide polymorphisms and ultrasensitive, massively parallel DNA sequencing now offer opportunities to detect somatic mutations in diseased tissue [33,44-46]. Such approaches could be leveraged to explore the possibility that sporadic cases of PHPV and perhaps other vitreoretinopathies are due to somatic mutation.

Beyond demonstrating the potential that somatic deletion of a single gene causes PHPV, our findings provide new insight into disease manifestations and the broader roles that $p19^{Arf}$ might play during mouse eye development. First, we previously demonstrated that the retrolental mass in *Arf* $^{-/-}$ animals usually becomes pigmented as the mice age [22,24]. In our current series of chimeric animals, the retrolental mass was composed of densely pigmented cells in nearly every case. Because the wild type lineage was albino, this allows us to conclude that the densely pigmented cells must be of *Arf* $^{-/-}$ origin. We do not know, though, whether this was due to selective migration of pigmented cells from the *Arf* $^{-/-}$ RPE or choroid, as implied by findings from the Nathans laboratory in *Fzd5* $^{-/-}$ mice [47]. It is also conceivable that the pigmented cells in the mass differentiate directly from non-pigmented, and primarily *Arf* $^{-/-}$ [25], cells populating the mass at birth. Regarding the latter concept, one might speculate that $p19^{Arf}$ may normally act to block melanocytic differentiation in the neural crest-derived cells that migrate to the developing primary vitreous.

We also previously showed that the relative contribution of wild type and *Arf* $^{-/-}$ cells in tail-derived DNA correlates closely with their contribution to the cornea and the RPE at birth [25]. This implies that $p19^{Arf}$ played no specific role in these tissues during development. In the 10-week-old chimeric animals studied here, the tail-derived DNA and RPE genotypes again correlated closely, but their correlation with the corneal epithelium was attenuated: The *Arf* $^{-/-}$ cells were underrepresented in the cornea in some cases and overrepresented in others. One straightforward explanation is that our one-dimensional analysis cannot reliably quantify cell lineage in the radially oriented cornea at 10 weeks, as opposed to the stippled lineage distribution in the newborn mouse [48]. Of note, we observed a relatively high intraclass correlation coefficient in the RPE and cornea analysis, and this finding helps to support the accuracy of our approach. Speculating that non-developmental factors control the relative number of wild type and *Arf* $^{-/-}$ cells in the cornea in older mice implies a functional role for $p19^{Arf}$ in this tissue. However, at least at the level of light microscopy, our studies of *Arf* $^{-/-}$ mice have failed to show corneal defects at any point through 10 weeks of age [22,24].

ACKNOWLEDGEMENTS

The authors gratefully acknowledge helpful comments from members of the Skapek laboratory. This work was supported by grants from the National Eye Institute to SXS (EY014368 and EY019942) and to the University of Tennessee Health Science Center (EY013080); and unrestricted grants to the Department of Ophthalmology at the University of Tennessee Health Science Center from Research to Prevent Blindness, Inc., New York, NY.

REFERENCES

1. Goldberg MF. Persistent fetal vasculature (PFV): an integrated interpretation of signs and symptoms associated with persistent hyperplastic primary vitreous (PHPV) LIV Edward Jackson Memorial Lecture. Am J Ophthalmol 1997; 124:587-626. [PMID: 9372715].
2. Ito M, Yoshioka M. Regression of the hyaloid vessels and pupillary membrane of the mouse. Anat Embryol (Berl) 1999; 200:403-11. [PMID: 10460477].
3. Haddad R, Font RL, Reeser F. Persistent hyperplastic primary vitreous. A clinicopathologic study of 62 cases and review of the literature. Surv Ophthalmol 1978; 23:123-34. [PMID: 100893].
4. Pollard ZF. Persistent hyperplastic primary vitreous: Diagnosis, treatment and results. Tr Am Ophth Coc1997. p. 487–549.
5. Hunt A, Rowe N, Lam A, Martin F. Outcomes in persistent hyperplastic primary vitreous. Br J Ophthalmol 2005; 89:859-63. [PMID: 15965167].
6. Lin AE, Biglan AW, Garver KL. Persistent hyperplastic primary vitreous with vertical transmission. Ophthalmol-PaediatrGenet. 1990; 11:121-2. [PMID: 2377350].
7. Wang MK, Phillips CI. Persistent hyperplastic primary vitreous in non-identical twins. Acta Ophthalmol (Copenh) 1973; 51:434-7. [PMID: 4800974].
8. Yu YS, Chang BL. Persistent hyperplastic primary vitreous in male twins. Korean J Ophthalmol 1997; 11:123-5. [PMID: 9510656].
9. Prasov L, Masud T, Khaliq S, Mehdi SQ, Abid A, Oliver ER, Silva ED, Lewanda A, Brodsky MC, Borchert M, Kelberman D, Sowden JC, Dattani MT, Glaser T. ATOH7 mutations cause autosomal recessive persistent hyperplasia of the primary vitreous. Hum Mol Genet 2012; 21:3681-94. [PMID: 22645276].
10. Okamoto N, Hatsukawa Y, Shimojima K, Yamamoto T. Submicroscopic deletion in 7q31 encompassing CADPS2 and TSPAN12 in a child with autism spectrum disorder and PHPV. Am J Med Genet A 2011; 155A:1568-73. [PMID: 21626674].
11. Su PH, Lee IC, Yang SF, Ng YY, Liu CS, Chen JY. Nine genes that may contribute to partial trisomy (6)(p22→pter) and unique presentation of persistent hyperplastic primary

vitreous with retinal detachment. Am J Med Genet A 2012; 158A:707-12. [PMID: 22407547].

12. Lobov IB, Rao S, Carroll TJ, Vallance JE, Ito M, Ondr JK, Kurup S, Glass DA, Patel MS, Shu W, Morrisey EE, McMahon AP, Karsenty G, Lang RA. Wnt7b mediates macrophage-induced programmed cell death in patterning the vasculature. Nature 2005; 437:417-21. [PMID: 16163358].

13. Gale NW, Thurston G, Hackett SF, Renard R, Wang Q, McClain J, Martin C, Witte C, Witte MH, Jackson D, Suri C, Campohiaro PA, Wiegand SJ, Yancopoulos GD. Angiopoietin-2 is required for postnatal angiogenesis and lymphatic patterning, and only the latter role is rescued by angiopoietin-1. Dev Cell 2002; 3:411-23. [PMID: 12361603].

14. Hackett SF, Wiegand S, Yancopoulos G, Campohiaro PA. Angiopoietin-2 plays an important role in retinal angiogenesis. J Cell Physiol 2002; 192:182-7. [PMID: 12115724].

15. Ikeda S, Hawes NL, Chang B, Avery CS, Smith RS, Nishina PM. Severe ocular abnormalities in C57BL/6 but not in 129/Sv p53-deficient mice. Invest Ophthalmol Vis Sci 1999; 40:1874-8. [PMID: 10393064].

16. Reichel MB, Ali RR, D'Esposito F, Clarke AR, Luther PJ, Bhattacharya SS, Hunt DM. High frequency of persistent hyperplastic primary vitreous and cataracts in p53-deficient mice. Cell Death Differ 1998; 5:156-62. [PMID: 10200460].

17. Saika S, Liu CY, Azhar M, Sanford LP, Doetschman T, Gendron RL, Kao CW, Kao WW. TGFbeta2 in corneal morphogenesis during mouse embryonic development. Dev Biol 2001; 240:419-32. [PMID: 11784073].

18. Ittner LM, Wurdak H, Schwerdtfeger K, Kunz T, Ille F, Leveen P, Hjalt TA, Suter U, Karlsson S, Hafezi F, Born W, Sommer L. Compound developmental eye disorders following inactivation of TGF· signaling in neural-crest stem cells. J Biol 2005; 4:11-[PMID: 16403239].

19. Freeman-Anderson NE, Zheng Y, Calla-Martin AC, Treanor LM, Zhao YD, Garfin PM, He TC, Mary MN, Thornton JD, Anderson C, Gibbons M, Saab R, Baumer SH, Cunningham JM, Skapek SX. Expression of the Arf tumor suppressor gene is controlled by Tgf{beta}2 during development. Development 2009; 136:2081-9. [PMID: 19465598].

20. Taharaguchi S, Yoshida K, Tomioka Y, Yoshino S, Uede T, Ono E. Persistent hyperplastic primary vitreous in transgenic mice expressing IE180 of the pseudorabies virus. Invest Ophthalmol Vis Sci 2005; 46:1551-6. [PMID: 15851549].

21. Rutland CS, Mitchell CA, Nasir M, Konerding MA, Drexler HCA. Microphthalmia, persistent hyperplastic hyaloid vasculature and lens anomalies following overexpression of VEGF-A 188 from the ‡A-crystallin promoter. Mol Vis 2007; 13:47-56. [PMID: 17277743].

22. McKeller RN, Fowler JL, Cunningham JJ, Warner N, Smeyne RJ, Zindy F, Skapek SX. The Arf tumor suppressor gene promotes hyaloid vascular regression during mouse eye development. Proc Natl Acad Sci USA 2002; 99:3848-53. [PMID: 11891301].

23. Silva RL, Thornton JD, Martin AC, Rehg JE, Bertwistle D, Zindy F, Skapek SX. Arf-dependent regulation of Pdgf signaling in perivascular cells in the developing mouse eye. EMBO J 2005; 24:2803-14. PMCID[PMID: 16037818].

24. Martin AC, Thornton JD, Liu J, Wang X, Zuo J, Jablonski MM, Chaum E, Zindy F, Skapek SX. Pathogenesis of persistent hyperplastic primary vitreous in mice lacking the arf tumor suppressor gene. Invest Ophthalmol Vis Sci 2004; 45:3387-96. [PMID: 15452040].

25. Thornton JD, Swanson DJ, Mary MN, Pei D, Martin AC, Pounds S, Goldowitz D, Skapek SX. Persistent hyperplastic primary vitreous due to somatic mosaic deletion of the arf tumor suppressor. Invest Ophthalmol Vis Sci 2007; 48:491-9. [PMID: 17251441].

26. Goldowitz D. The weaver granuloprival phenotype is due to intrinsic action of the mutant locus in granule cells: evidence from homozygous weaver chimeras. Neuron 1989; 2:1565-75. [PMID: 2627379].

27. Jablonski MM, Dalke C, Wang X, Lu L, Manly KF, Pretsch W, Favor J, Pardue MT, Rinchik EM, Williams RW, Goldowitz D, Graw J. An ENU-induced mutation in Rs1h causes disruption of retinal structure and function. Mol Vis 2005; 11:569-81. [PMID: 16088326].

28. Cuzick J. A Wilcoxon-type test for trend. Stat Med 1985; 4:87-90. [PMID: 3992076].

29. Khaliq S, Hameed A, Ismail M, Anwar K, Leroy B, Payne AM, Bhattacharya SS, Mehdi SQ. Locus for autosomal recessive nonsyndromic persistent hyperplastic primary vitreous. Invest Ophthalmol Vis Sci 2001; 42:2225-8. [PMID: 11527934].

30. Zheng Y, Zhao YD, Gibbons M, Abramova T, Chu PY, Ash JD, Cunningham JM, Skapek SX. Tgfbeta signaling directly induces Arf promoter remodeling by a mechanism involving Smads 2/3 and p38 MAPK. J Biol Chem 2010; 285:35654-64. [PMID: 20826783].

31. Sherr CJ. The Ink4a/Arf network in tumour suppression. Nat Rev Mol Cell Biol 2001; 2:731-7. [PMID: 11584300].

32. Zindy F, Williams RT, Baudino TA, Rehg JE, Skapek SX, Cleveland JL, Roussel MF, Sherr CJ. Arf tumor suppressor promoter monitors latent oncogenic signals in vivo. Proc Natl Acad Sci USA 2003; 100:15930-5. [PMID: 14665695].

33. Prochazkova K, Pavlikova K, Minarik M, Sumerauer D, Kodet R, Sedlacek Z. Somatic TP53 mutation mosaicism in a patient with Li-Fraumeni syndrome. Am J Med Genet A 2009; 149A:206-11. [PMID: 19012332].

34. Hewitt C, Wu CL, Evans G, Howell A, Elles RG, Jordan R, Sloan P, Read AP, Thakker N. Germline mutation of ARF in a melanoma kindred. Hum Mol Genet 2002; 11:1273-9. [PMID: 12019208].

35. Randerson-Moor JA, Harland M, Williams S, Cuthbert-Heavens D, Sheridan E, Aveyard J, Sibley K, Whitaker L, Knowles M, Bishop JN, Bishop DT. A germline deletion of p14Arf but not CDKN2A in a melanoma-neural system

tumour syndrome family. Hum Mol Genet 2001; 10:55-62. [PMID: 11136714].

36. Laud K, Marian C, Avril MF, Barrois M, Chompret AM, Tucker MA, Clark PA, Peters G, Chaudru V, Demenais F, Spatz A, Smith MW, Lenoir GM, Bressa-de Paillerets B. Comprehensive analysis of CDKN2A (p16Ink4a/p14ARF) and CDKN2B genes in 53 melanoma index cases considered to be at heightened risk of melanoma. J Med Genet 2006; 43:39-47. [PMID: 15937071].

37. Gil J, Peters G. Regulation of the INK4b-ARF-INK4a tumour suppressor locus: all for one or one for all. Nat Rev Mol Cell Biol 2006; 7:667-77. [PMID: 16921403].

38. DiCiommo D, Gallie BL, Bremner R. Retinoblastoma: the disease, gene and protein provide critical leads to understand cancer. Semin Cancer Biol 2000; 10:255-69. [PMID: 10966849].

39. Kamijo T, Zindy F, Roussel MF, Quelle DE, Downing JR, Ashmun RA, Grosveld G, Sherr CJ. Tumor suppression at the mouse INK4a locus mediated by the alternative reading frame product p19ARF. Cell 1997; 91:649-59. [PMID: 9393858].

40. Kamijo T, Bodner S, van de Kamp E, Randle DH, Sherr CJ. Tumor spectrum in ARF-deficient mice. Cancer Res 1999; 59:2217-22. [PMID: 10232611].

41. Eischen CM, Weber JD, Roussel MF, Sherr CJ, Cleveland JL. Disruption of the ARF-Mdm2-p53 tumor suppressor pathway in Myc-induced lymphomagenesis. Genes Dev 1999; 13:2658-69. [PMID: 10541552].

42. Gardie B, Cayuela JM, Martini S, Sigaux F. Genomic alterations of the p19Arf encoding exons in T-cell acute lymphoblastic leukemia. Blood 1998; 91:1016-20. [PMID: 9446664].

43. Wu CL, Roz L, McKown S, Sloan P, Read AP, Holland S, Porter S, Scully C, Paterson I, Tavassoli M, Thakker N. DNA studies underestimate the major role of CDKN2A inactivation in oral and oropharyngeal squamous cell carcinomas. Genes Chromosomes Cancer 1999; 25:16-25. [PMID: 10221335].

44. Laurie CC, Laurie CA, Rice K, Doheny KF, Zelnick LR, McHugh CP, Ling H, Hetrick KN, Pugh EW, Amos C, Wei Q, Wang LE, Lee JE, Barnes KC, Hansel NN, Mathias R, Daley D, Beaty TH, Scott AF, Ruczinski I, Scharpf RB, Bierut LJ, Hartz SM, Landi MT, Freedman ND, Goldin LR, Ginsburg D, Li J, Desch KC, Strom SS, Blot WJ, Signorello LB, Ingles SA, Chanock SJ, Berndt SI, Le Marchand L, Henderson BE, Monroe KR, Heit JA, de Andrade M, Armasu SM, Regnier C, Lowe WL, Hayes MG, Marazita ML, Feingold E, Murray JC, Melbye M, Feenstra B, Kang JH, Wiggs JL, Jarvik GP, McDavid AN, Seshan VE, Mirel DB, Crenshaw A, Sharopova N, Wise A, Shen J, Crosslin DR, Levine DM, Zheng X, Udren JI, Bennett S, Nelson SC, Gogarten SM, Conomos MP, Heagerty P, Manolio T, Pasquale LR, Haiman CA, Caporaso N, Weir BS. Detectable clonal mosaicism from birth to old age and its relationship to cancer. Nat Genet 2012; 44:642-50. [PMID: 22561516].

45. Macosko EZ, McCarroll SA. Exploring the variation within. Nat Genet 2012; 44:614-6. [PMID: 22641203].

46. Poduri A, Evrony GD, Cai X, Walsh CA. Somatic mutation, genomic variation, and neurological disease. Science 2013; 341:1237758-[PMID: 23828942].

47. Liu C, Nathans J. An essential role for frizzled 5 in mammalian ocular development. Development 2008; 135:3567-76. [PMID: 18832390].

48. Collinson JM, Hill RE, West JD. Analysis of mouse eye development with chimeras and mosaics. Int J Dev Biol 2004; 48:793-804. [PMID: 15558472].

Articles are provided courtesy of Emory University and the Zhongshan Ophthalmic Center, Sun Yat-sen University, P.R. China. The print version of this article was created on 3 March 2014. This reflects all typographical corrections and errata to the article through that date. Details of any changes may be found in the online version of the article.